中國土木水利工程學刊 第三十三卷 第一期 (民國一一〇年)
Journal of the Chinese Institute of Civil and Hydraulic Engineering, Vol. 33, No. 1, pp. 001–010, 2021
DOI : 10.6652/JoCICHE.202103_33(1).0001

NONLINEAR FAILURE ANALYSIS OF FIBER-REINFORCED COMPOSITE LAMINATES SUBJECTED TO PIN STRESS AND WASHER CLAMPING PRESSURE

Teng-Chun Yang

Department of Forestry
National Chung Hsing University
Taichung, Taiwan 40227, R.O.C.

Shu-Wei Chang

YangMei Laboratory
Testing Department 1
CECI Nova Technology Co., Ltd.,
Taoyuan, Taiwan 326, R.O.C.

Hsuan-Teh Hu

Department of Civil Engineering
National Cheng Kung University
Tainan, Taiwan 70101, R.O.C.

Department of Civil and Disaster Prevention Engineering
National United University
Miaoli, Taiwan 36063, R.O.C.

Key Words: composite laminate, pin stress, washer clamping pressure, nonlinear failure analysis.

ABSTRACT

In this study, the nonlinear model was used to predict the failure loads of fiber-reinforced composite laminates subjected to pin stress and washer clamping pressure. The nonlinear model included nonlinear constitutive law, mixed failure mode composed of the Tsai-Wu and maximum stress criteria, and post failure response. Appropriate constitutive models were established using the software ABAQUS, and the numerical analysis and the experimental data were compared. The results showed that the proposed model could accurately simulate nonlinear material behavior of composite laminates. In addition, parametric studies for effects of laminate layup, geometric variables, washer size and clamping pressure on the failure load of composite laminates with a pin/washer loaded joint were presented.

纖維複合材料疊層板受螺栓應力及墊圈夾壓下之非線性破壞分析

楊登鈞[1] 張書維[2] 胡宣德[3*]

關鍵詞：複合疊層板，螺栓應力，墊圈夾壓，非線性破壞分析。

摘 要

本研究使用非線性模型，對纖維複合材疊層板受螺栓應力及墊圈夾壓下，進行板材之破壞預測及數值分析。此模型包含非線性組成律、混合破壞準則 (Tsai-Wu 破壞準則與最大應力準則) 及後破壞分析模式。本研究使用 ABAQUS 軟體建立適當的組成模型，並將數值分析與實驗數據比較。結果發現，本研究建議的非線性組成模型與分析模式，準確模擬纖維複合材疊層板之非線性行為。此外，對纖維複合材疊層板受到螺栓應力及墊圈夾壓情況下，進行板材不同疊序、幾何圖形及墊圈夾壓力等參數研討，除探討數值分析結果外並做綜合之討論。

[1] 國立中興大學森林學系副教授

[2] 華光工程顧問股份有限公司試驗一部楊梅試驗室

[3] *通訊作者，國立成功大學土木工程學系特聘教授暨國立聯合大學副校長

1. INTRODUCTION

Recently, fiber-reinforced plastic composites (FRPCs) have been used widely used in aerospace industry, automotive, and civil engineering due to light weight and high mechanical properties. Generally, a FRPC laminate in service is drilled the hole for bolt joints to facility to its assemble or disassemble, as well as applications for transferring loads between structural components [1]. However, the bolt-jointed composite laminates are accompanied with stress concentration of a pin and bypass loading of washers surrounding the hole to cause the reduction in the load carrying ability of their structure. In the past two decades, a major of researches have focused on the evaluation of joint's strength and the prediction of its failure mechanism of composite laminates with pin-loaded joint. Collings [2] and Kretsis and Matthews [3] reported that the magnitude of initial clamping force has a significant effect to shift the failure mechanism and the sequence where this failure appears and suppresses the failure response near joints of composite laminates. An extensive list of pertinent publications was provided by the review papers of Thoppul et al. [4] and Camando and Matthews [5]. In recent years, some studies improved and proposed the numerical models to accurately predict the failure strength or the failure mechanism of composite laminates with pin stress [6-10] and/or washer clamping pressure [11-13]. As mentioned above, the investigation of the failure behavior of pin-loaded composite laminates with clamping pressure have been received considerable attention and most critical. Lin and Hu [14,15] verified that the nonlinear models, including stress-strain relations, mixed failure composed of the Tsai-Wu, maximum stress criteria, and post failure response, were applicable for simulating the nonlinear behavior of a FRPC subjected to uniaxial or biaxial tensile load. Hu et al. [16] reported that this proposed material constitutive models were proved to correctly simulate the nonlinear behavior of composite skew plates under uniaxial compressive force. On the other hand, a few studies explored to accurately predict the nonlinear behavior of a FRPC, which was used for strengthening square reinforced concrete plates [17-19]. To date, there is little information available simulations on determining the damage behavior of individual lamina in the composite laminate with a pin/washer-loaded joint using the proposed nonlinear analysis model, including stress-strain relations, mixed failure criteria, and post failure response. Therefore, a main objective of this present study was to evaluate the capability and generality of the proposed models using the ABAQUS finite element program [20] for the nonlinear analysis of FRPC with pin-filled hole subjected pin stress and washer clamping pressure. Additionally, the models were validated with the experimental results of Okutan [21] and Hung and Chang [22]. Furthermore, a series of numerical analyses were demonstrated to investigate the influences of laminate layups, geometric variables, and washer clamping pressure on the failure load of composite laminates with a pin/washer-loaded joint.

2. NONLINEAR FINITE ELEMENT MODEL

The finite element software package (ABAQUS program) was used to carry out the numerical analyses of a FRPC [20]. In this the software simulation, the constitutive models to simulate the entire load-displacement behavior of a FRPC were employed. On the other hand, the reliable nonlinear material model for a FRPC was implemented into a FORTRAN subroutine and linked to the ABAQUS finite element program, including nonlinear constitutive law, mixed failure criterion and post failure mode.

2.1 Modeling of Laminate, Pin and Washer

Each FRPC lamina was considered as an orthotropic layer (Fig. 1). In in-plane shear stress–strain relation, it is observed that the nonlinearity of the unidirectional fibrous composite subjected to in-plane transverse loading. However, the degree of nonlinearity is not comparable to the deviation from linearity in the in-plane shear [23]. Therefore, Jones and Morgan [24] reported that this nonlinearity, which is associated with the transverse loading, can be negligible. Accordingly, the nonlinear strain-stress relation to model the nonlinear in-plane shear behavior of a composite lamina is shown by [23]:

$$\begin{Bmatrix}\varepsilon_1\\ \varepsilon_2\\ \gamma_{12}\end{Bmatrix}=\begin{bmatrix}\frac{1}{E_{11}} & -\frac{\nu_{21}}{E_{22}} & 0\\ -\frac{\nu_{12}}{E_{22}} & \frac{1}{E_{22}} & 0\\ 0 & 0 & \frac{1}{G_{12}}\end{bmatrix}\begin{Bmatrix}\sigma_1\\ \sigma_2\\ \tau_{12}\end{Bmatrix}+S_{6666}\tau_{12}^2\begin{Bmatrix}0\\ 0\\ \tau_{12}\end{Bmatrix} \quad (1)$$

where S_{6666} is the in-plane shear nonlinearity, which is one constant that is determined by a curve fit to various off-axis tension test data [23]. In the constitutive equations of the lamina, its increment of stress-strain relations ($\Delta\{\sigma'\}$) and transverse shear stresses ($\Delta\{\tau_t'\}$) can be written as:

$$\Delta\{\sigma'\}=[Q_1']\,\Delta\{\varepsilon'\},\ \ \Delta\{\tau_t'\}=[Q_t']\,\Delta\{\gamma_t'\} \quad (2)$$

where $\Delta\{\sigma'\}=\Delta\{\sigma_1,\sigma_2,\sigma_{12}\}^T$, $\Delta\{\varepsilon'\}=\Delta\{\varepsilon_1,\varepsilon_2,\varepsilon_{12}\}^T$, $\Delta\{\tau_t'\}=\Delta\{\tau_{13},\tau_{23}\}^T$, $\Delta\{\gamma_t'\}=\Delta\{\gamma_{13},\gamma_{23}\}^T$, and

$$[Q_1']=\begin{bmatrix}\frac{E_{11}}{1-\nu_{12}\nu_{21}} & \frac{\nu_{12}E_{22}}{1-\nu_{12}\nu_{21}} & 0\\ \frac{\nu_{21}E_{11}}{1-\nu_{12}\nu_{21}} & \frac{E_{22}}{1-\nu_{12}\nu_{21}} & 0\\ 0 & 0 & \frac{1}{1/G_{12}+3S_{6666}\tau_{12}^2}\end{bmatrix},$$

$$[Q_2']=\begin{bmatrix}\alpha_1 G_{13} & 0\\ 0 & \alpha_2 G_{23}\end{bmatrix} \quad (3)$$

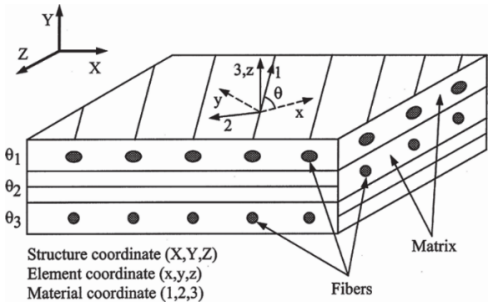

Fig. 1 Material, element, and structure coordinates of a FRCP laminate

The $[Q_1']$ and $[Q_2']$ are inverse matrices of each equations. The α_1 and α_2 are shear correction factors and taken to be 0.83 in this study.

Before assembling the stiffness matrices from element level to global level, the constitutive matrices of composite materials at element integration points must be calculated. For fiber-composite materials, the increment of constitutive equations of a lamina in the element coordinates (x, y, z) can be written as:

$$\Delta\{\sigma\} = [Q_1]\,\Delta\{\varepsilon\},\ \Delta\{\tau_t\} = [Q_2]\,\Delta\{\gamma_t\} \tag{4}$$

where

$\Delta\{\sigma\} = \Delta\{\sigma_x,\ \sigma_y,\ \sigma_{xy}\}^T$, $\Delta\{\varepsilon\} = \Delta\{\varepsilon_x,\ \varepsilon_y,\ \varepsilon_{xy}\}^T$, $\Delta\{\tau_t\} = \Delta\{\tau_{xz},\ \tau_{yz}\}^T$, $\Delta\{\gamma_t\} = \Delta\{\gamma_{xz},\ \gamma_{yz}\}^T$, and

$$[Q_1] = [T_1]^T[Q_1'][T_2],\ [Q_2] = [T_2]^T[Q_2'][T_2] \tag{5}$$

$$[T_1] = \begin{bmatrix} \cos^2\theta & \sin^2\theta & \sin\theta\cos\theta \\ \sin^2\theta & \cos^2\theta & -\sin\theta\ \cos\theta \\ -2\sin\theta\cos\theta & 2\sin\theta\cos\theta & \cos^2\theta-\sin^2\theta \end{bmatrix},$$

$$[T_2] = \begin{bmatrix} \cos\theta & \sin\theta \\ -\sin\theta & \cos\theta \end{bmatrix} \tag{6}$$

The θ in Eq. (6) is measured counterclockwise from the element local x-axis to the material 1-axis (Fig. 1).

For failure criteria, the Tsai-Wu criterion [25] is adopted in this study. This failure criterion under plane stress conditions has the following form:

$$F_1\sigma_1 + F_2\sigma_2 + F_{11}\sigma_1^2 + F_{12}\sigma_1\sigma_2 + F_{22}\sigma_2^2 + F_{66}\sigma_{12}^2 = 1 \tag{7}$$

with

$$F_1 = \frac{1}{\bar{X}} + \frac{1}{\bar{X}'},\quad F_2 = \frac{1}{\bar{Y}} + \frac{1}{\bar{Y}'},\quad F_{11} = \frac{1}{\bar{X}\bar{X}'},\quad F_{11} = \frac{1}{\bar{Y}\bar{Y}'},$$
$$F_{66} = \frac{1}{\bar{S}^2}$$

The $\bar{X}$ and $\bar{X}'$ are the longitudinal strengths of the lamina in tension and compression. The $\bar{Y}$ and $\bar{Y}'$ are the transverse strengths of the lamina in tension and compression. The $\bar{S}$ is shear strength of the lamina. For the stress interaction term, F_{12}, which is equal to zero for practical engineering application [26]. According to Eq. (3), it has indicated incremental loading is applied to composite plates until failures in one or more of individual plies. However, the failure mode are not distinguished in Tsai-Wu criterion. Therefore, the following two rules are used to determine the ply failure that is caused by resin fracture or fiber breakage [27]:

(1) If σ_1 exceeds the uniaxial strength of the lamina, i.e. $\sigma_1 \ge \bar{X}$ or $\sigma_1 \le \bar{X}'$, the ply failure is caused by the fiber breakage and it assumed a total ply rupture. The constitutive matrix of the lamina is expressed as:

$$[Q_1'] = \begin{bmatrix} 0 & 0 & 0 \\ 0 & 0 & 0 \\ 0 & 0 & 0 \end{bmatrix} \tag{8}$$

(2) If σ_1 exhibits less than the uniaxial strength of the lamina in the fiber direction, i.e. $\bar{X}' \le \sigma_1 \le \bar{X}$, the ply failure is assumed to be resin induced. The constitutive matrix of the lamina is written as:

$$[Q_1'] = \begin{bmatrix} E_{11} & 0 & 0 \\ 0 & 0 & 0 \\ 0 & 0 & 0 \end{bmatrix} \tag{9}$$

The laminated shells are modeled by eight-node isoparametric shell elements with six degrees of freedom per note, including three displacements and three rotations in the finite element analysis. The element stiffness matrix is formulated by employing the reduced integration rule together with hourglass stiffness. For modeling of a pin and a washer, they both are assumed as rigid body, and twenty-node isoparametric solid elements with three degrees of freedom (three displacements) per note are used.

2.2 Geometrical Modeling

In order to simulate the practical application, all geometrical modeling including one composite laminate, one pin and two washers were established. Sizes of a laminate, pin, and washer are defined as shown in Fig. 2, where L is the length, W is the width, t is the lamina thickness, D is the diameter of a hole, D_w is the diameter of a washer, and E is the distance from the free edge of the composite. The analyzed composite laminates with one pin and two washers were set according to boundary conditions as shown in Fig. 3. The fiber orientation of the laminate can be selected arbitrarily, but it must be symmetric for the middle plane of the plate. The laminate is subjected to uniaxial tensile load only (Fig. 3), and it is not applied by out-of plane loading, bending or torsion. The laminate is assumed to be perfectly bounded, and no slipping occurs within the laminate. Eight node shell elements are used to simulate the laminate in the numerical analysis. ABAQUS program can automatically transform the local stresses and strains of the shell element in each lamina to global coordinates

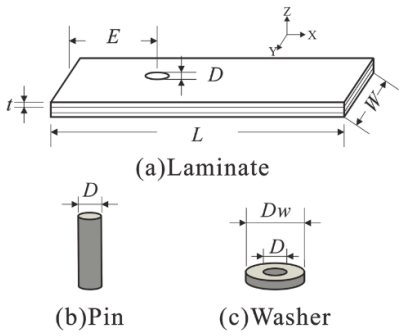

Fig. 2 Geometric conditions of the composite laminate (a), the pin (b), and the washer (c)

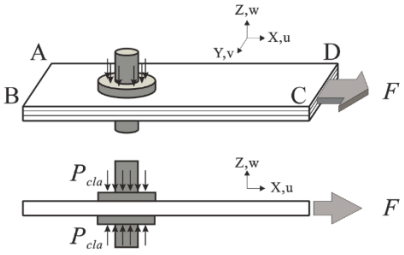

Boundary conditions:

w = 0	on sides of AB, BC, and AD
v = w = 0	on the side of CD
u = v = 0	around inner diameter of the washer
u = v = w =0	on the top and bottom of the pin

Fig. 3 Boundary conditions of the composite laminates subjected to tensile force (F) and washer clamping pressure (P_{cla})

(Fig. 1). Basically, each incremental step calculates stresses and strains, and the occurrence of failure and the mode of failure were determined by the failure criteria. According to the property degradation of models, mechanical properties in the damaged area reduce appropriately. Any additional damage will be determined by recalculated stresses and strains as a result of stress redistribution at the same load. When the laminates cannot sustain any additional load, the final failure load is determined.

3. VERIFICATION OF THE PROPOSED MODEL

In order to verify the proposed nonlinear failure analysis model, numerical results generated from the model are compared with the test data measured from two experiments [21,22]. One of the experimental data for a pin-loaded composite laminate was taken from Okutan [21]. The other for a pin/washer-loaded composite laminate was taken from Hung and Chang [22]. Hence, two systems, including a pin-loaded composite and a pin/washer-loaded composite, were set up to verify the proposed nonlinear failure analysis model and conduct parametric studies.

In the following, the numerical result in terms of the failure load carrying capacities and load-displacement relations. The results of the comparison are presented as follows:

3.1 Composite Laminates with a Pin-loaded Joint

A typical finite element mesh of a composite laminate with hole is shown in Fig. 4(a). A large number of elements at the edge of the hole was set to obtain a better accuracy of the stresses. Comparisons on load-displacement relations between the predictions and the experimental data of $[0/90/0]_s$ and $[90/0/90]_s$ for different width/diameter (W/D) and edge distance/diameter (E/D) are presented in Fig. 5. The experimental data obtained from Okutan [21] was compared with the predications based on the model in this study. The material was a glass-fiber/epoxy composite, and a laminate

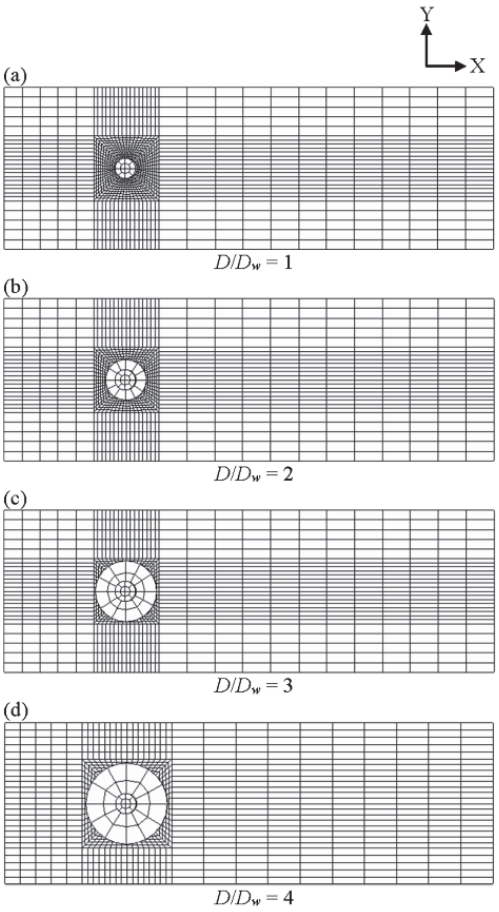

Fig. 4 A typical finite element mesh of a laminate with pin-filled hole and different washer size (D_w/D)

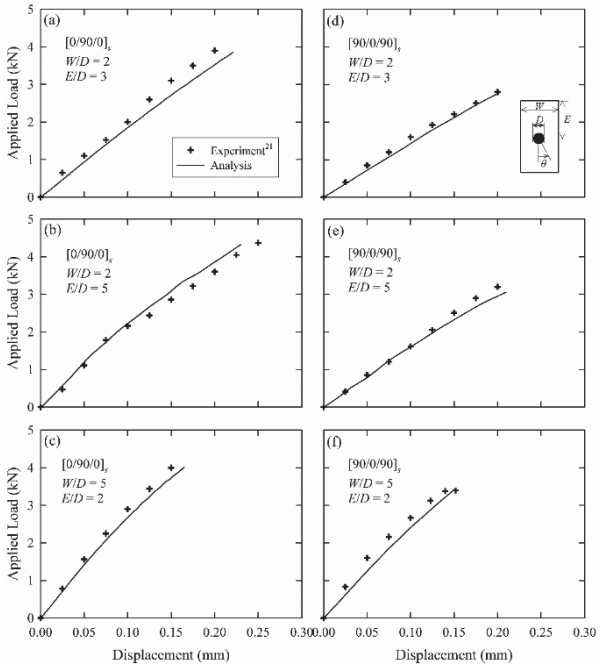

Fig. 5 Comparisons on load-displacement relations of composite laminates with a pin-loaded joint between the predictions and the experimental data [21]

length (L), a lamina thickness (t) and hole diameter (D) were fixed to 5 cm, 0.055 cm, and 0.5 cm, respectively. The material properties and strengths of this composite is summarized in Table 1. The coefficient of friction between the pin and the laminate was assumed to be 0.2 for the calculations. Overall, the predictions agreed with the experimental test data very well. Additionally, the results exhibited that the failure load and the load-displacement relations of all layup composite laminates were in good agreement with experimental data. The error for failure loads between the prediction and the experimental data was about 3% ~ 5%.

The validity of the proposed model for effects of E/D on three failure modes of $[0/90/0]_s$ and $[90/0/90]_s$ with fixed 2 of W/D as compared to the experimental test and the analysis obtained from Okutan [21] is shown in Fig. 6. The net-tension stress ($\sigma_{NT} = F_f/(W - D)t_c$) is defined as the failure load (F_f) divided by the width subtracted the hole diameter and the composite laminate thickness (t_c); the shearing stress ($\sigma_{SR} = F_f/Et_c$) is defined as the failure load divided by the distance of the edge and the composite laminate thickness; the bearing stress ($\sigma_{BR} = F_f/Dt_c$) is defined as the failure load divided by the hole diameter and the composite laminate thickness. These failure modes have been observed experimentally that mechanically fastened joints fail, including net-tension, shear-out, and bearing. Typical damage mechanism due to each modes is shown in Fig. 7. The parameters of the materials properties, geometrical dimensions, and laminate configurations can affect the failure load, mechanism of failure, the position of the initial failure, and the magnitude of the first ply failure load. The results exhibited that the three predicted failure stresses for $[0/90/0]_s$ and $[90/0/90]_s$ were in a great agreement with the experimental data within 10% error. Furthermore, the prediction showed much better fit than the analysis obtained from the literature [21]. The calculation verified that the proposed laminate model in this study is applicable for the laminate with a pin-loaded joint subjected to tensile stress.

Table 1 Material properties of composites used in the calculations

Material properties	Glass-fiber/epoxy [21]	T800H/3900-2 [22]
Moduli		
Longitudinal Young's modulus, E_{11} (GPa)	44	160
Transverse Young's modulus, E_{22} (GPa)	10.5	9.0
In-plane shear modulus, G_{12} (GPa)	3.7	6.2
Poisson's ratio, ν_{12}	0.36	0.28
Shear nonlinearity parameter, S_{6666} (GPa)$^{-3}$	71.7	30.5
Strengths		
Longitudinal tensile strength, $\bar{X}$ (MPa)	800	2840
Longitudinal compressive strength, $\bar{X}'$ (MPa)	− 350	− 1551
Transverse tensile strength, $\bar{Y}$ (MPa)	50	44
Transverse compressive strength, $\bar{Y}'$ (MPa)	− 125	− 168
Shear strength, $\bar{S}$ (MPa)	120	365

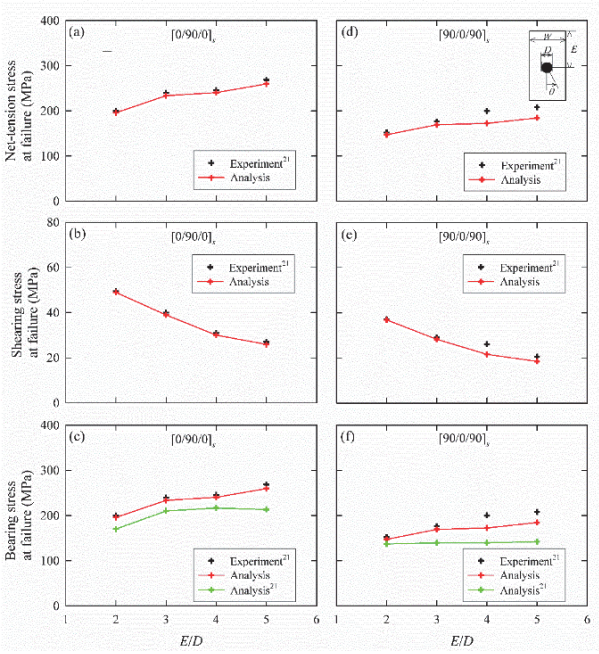

Fig. 6 Three failure modes with various E/D for $[0/90/0]_s$ and $[90/0/90]_s$ composite laminates with a pin-loaded joint ($W/D = 2$)

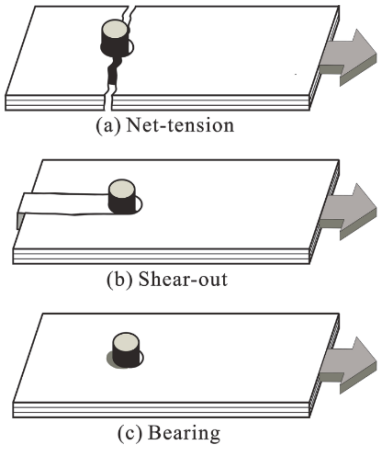

Fig. 7 Typical failure modes of the composite laminates with a pin-loaded joint

3.2 Composite Laminates with Pin/Washer-loaded Joints

In order to verify the feasibility of the proposed laminate model for the laminate with pin-filled hole subjected to tensile stress and washer clamping pressure, the experimental data obtained from Hung and Chang [22] were compared with the predications based on the model in this study. A typical finite element mesh of a laminate with pin-filled hole and different

washer size (D_w/D) is shown in Figs. 4(b) to 4(d). Lots of elements was set around the hole and washer clamping area to obtain a better accuracy of the stresses. According to the literature [22], in order to ensure that the fracture of the laminate in bearing mode, the geometry with 8 of W/D and 6 of E/D was selected. The initial clamping pressure (P_{cla}) was calculated to the failure load (F_f) divided by the washer area (A_w). The coefficient of friction between the washer and the laminate was assumed to be 0.15 for the calculations. The material was a T800H/3900-2 composite, and a laminate length (L), a lamina thickness (t), and hole diameter (D) were fixed to 15.24 cm, 0.016 cm and 0.635 cm, respectively. As shown in Fig. 8, the predicted and the measured failure loads of $[0/90]_{6s}$ and $[90/\pm45/0]_{3s}$ with pin/washer-loaded joints as a function of P_{cla} are presented. The outer diameter of a washer was twice of the hole diameter ($D_w/D = 2$). For $[0/90]_{6s}$ with 5.5 MPa of P_{cla}, it exhibited that the present analysis was recorded at around 18.9 kN of F_f, and it was in agreement with the experimental 17.8 kN of F_f with an error of 6.2%. Compared of the F_f of the experimental test and the present analysis of quasi-isotropic $[90/\pm45/0]_{3s}$ with 44.1 MPa of P_{cla}. The F_f of this layup composite laminate was recorded 26.1 kN of F_f in good agreement with 25.7 kN of F_f at experimental data. The error was about 1.6%.

Figure 9 shows the bearing stress of $[0/90]_{6s}$ and $[90/\pm45/0]_{3s}$ with pin/washer joints as a function of the initial P_{cla}. Except for $[90/\pm45/0]_{3s}$ with the smaller P_{cla} ($\leq$ 5 MPa), the predicted bearing stress were very close to the experimental data and the analysis obtained from the literature [22]. Generally, the smaller P_{cla} ($\leq$ 5 MPa) is equivalent to finger-tight pressure. In this study, using the proposed nonlinear analysis, the predicted bearing stress of the laminate with the specific layout and the smaller P_{cla} showed underestimation as compared to the analysis [22] and the experimental data [22]. In the future, the aim of our study is to further improve the proposed model and simulate for the nonlinear behavior of the composite laminate with the smaller P_{cla}. Overall, the results verified that the proposed materials model are satisfactory in the laminate with pin-filled hole subjected to tensile stress and the lager washer clamping pressure (> 5 MPa).

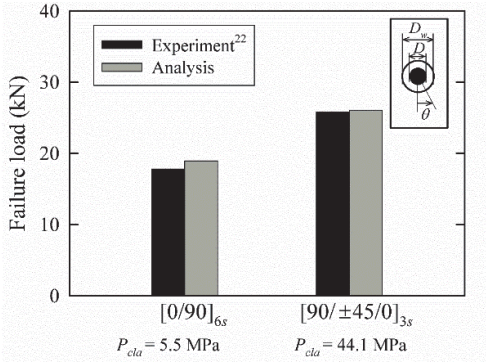

Fig. 8 Comparisons on failure loads of composite laminates with pin/washer-loaded joints between the predictions and the experimental data [22] ($W/D = 8$, $E/D = 6$, $D_w/D = 2$)

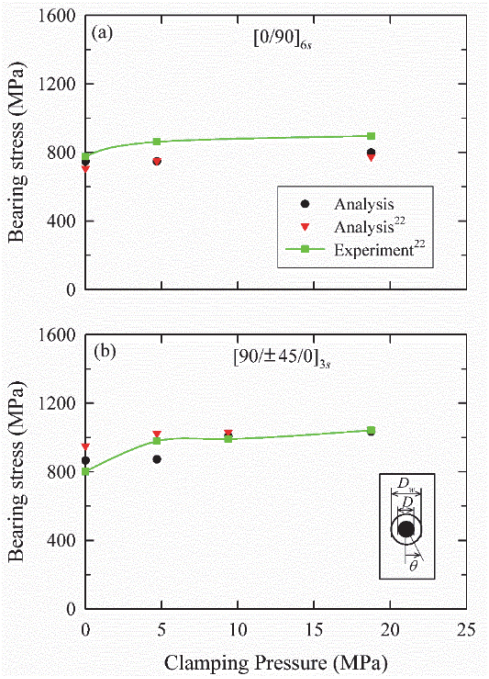

Fig. 9 Bearing stress of composite laminates with pin/washer-loaded joints as a function of the initial clamping pressure ($W/D = 8$, $E/D = 6$)

4. PARAMETRIC STUDIES

4.1 Effects of Dimension Ratios on Composite Laminates with a Pin-loaded Joint

Figures 10 to 13 show effects of dimension ratios on stress-strain relations of cross-ply and angle-ply composite laminates with a pin-loaded joint. Therein, net-tension stress (σ_{NT}) and strain (ε) were calculated below:

$$\sigma_{NT} = \frac{F}{(W-D)t_c}, \varepsilon = \frac{\Delta}{L} \tag{10}$$

where F is applied load; W is the width of a composite laminate; D is the diameter of the hole; t_c is thickness of a composite laminate; Δ is the stretched displacement of a composite laminate under tensile force; L is the length of a composite laminate. For cross-ply $[(\theta/\theta-90)_2]_s$ with fixed 5 of E/D (Fig. 10), all stress-strain curves of composite laminates with the same fiber angle (θ) exhibited the same tendency, which the net-tension at failure (σ_{NTf}) and strain at failure (ε_f) both decreased with the increase in W/D. In addition, the linear stress-strain curves occurred at cross-ply composite laminates with the smaller θ (say $\theta < 30°$), while the nonlinear curves were observed when θ was above 30°, especially for $[(45/-45)_2]_s$. For angle-ply $[(\theta/-\theta)_2]_s$ with fixed E/D, the linear curves were observed when the θ was below 45°, and the σ_{NTf} and ε_f decreased with the decrease in W/D (Fig. 11(a) and 11(b)). At 45° of θ, it was observed that the same trend can be found to the obvious nonlinear curves (Fig. 10(d)). Above 45° of θ (Figs. 11(c) and 11(d)), although the ε_f performed irregular, the σ_{NTf}

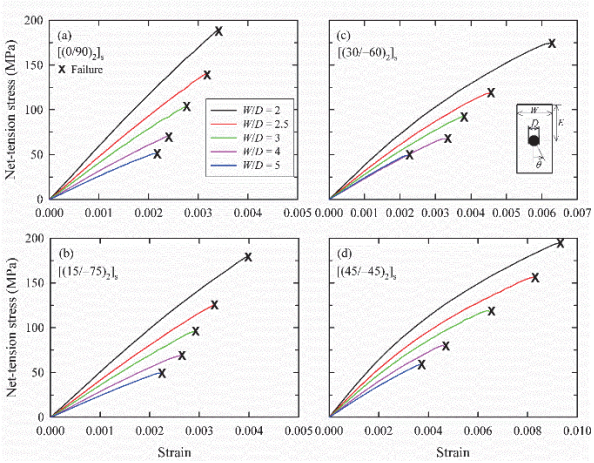

Fig. 10 Effect of *W*/*D* on stress-strain curves of cross-ply composite laminates with a pin-loaded joint (*E*/*D* = 5)

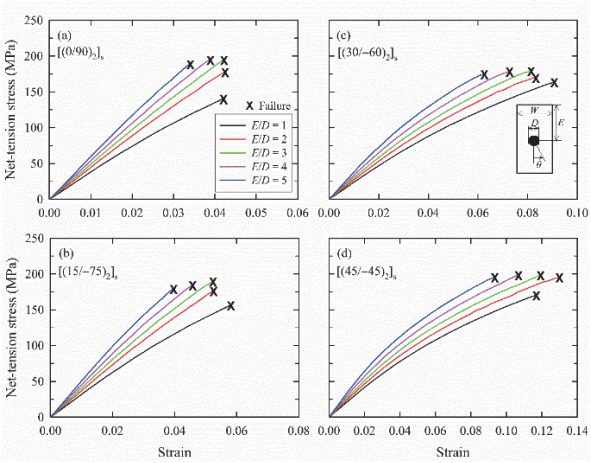

Fig. 12 Effect of *E*/*D* on stress-strain curves of cross-ply composite laminates with a pin-loaded joint (*W*/*D* = 2)

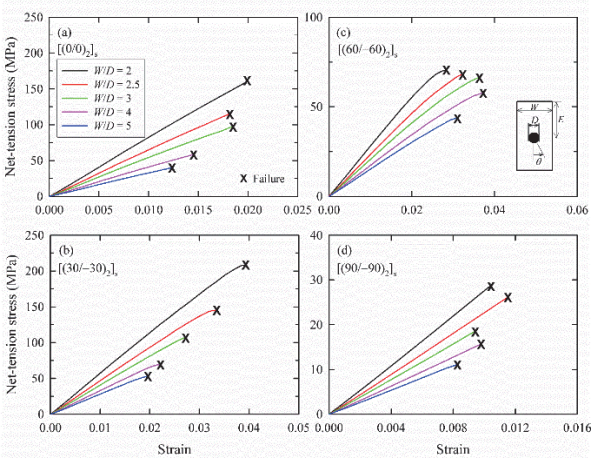

Fig. 11 Effect of *W*/*D* on stress-strain curves of angle-ply composite laminates with a pin-loaded joint (*E*/*D* = 5)

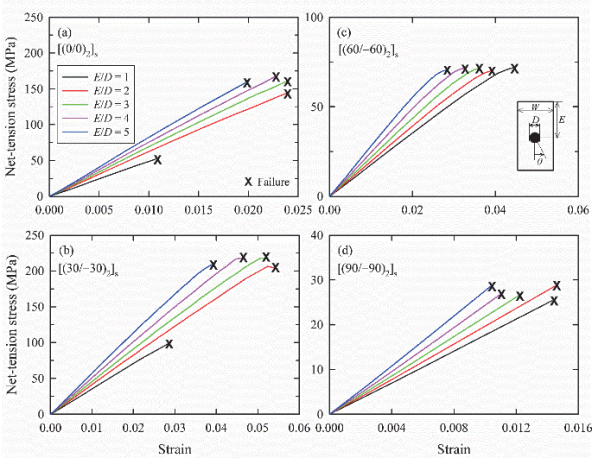

Fig. 13 Effect of *E*/*D* on stress-strain curves of angle-ply composite laminates with a pin-loaded joint (*W*/*D* = 2)

decreased with the increase in *W*/*D*. Furthermore, it can be seen that the σ_{NTf} of $[(60/-60)_2]_s$ and $[(90/-90)_2]_s$ were recorded to 40 ~ 75 MPa and 10 ~ 30 MPa, respectively. The phenomena can be explained that the more portion of matrix in the composite laminate resists tensile direction, and it has been well-known that the tensile resistance of matrix is extremely weak than that of fiber. As shown in Fig. 12, it can be seen that the σ_{NTf} of all cross-ply composite laminates with 1 of *E*/*D* was the smallest. However, when *E*/*D* was above 1, no significant difference for the σ_{NTf} of all cross-ply composite laminates was observed, but this value fell inside the range of 150 ~ 200 MPa. In the following, Fig. 13 illustrated that effects of *E*/*D* on stress-strain curves of angle-ply composite laminates with a pin-loaded joint. When θ was below 45°, it was also observed that the σ_{NTf} and ε_f of laminates with 1 of *E*/*D* were both the smallest. However, when *E*/*D* was above 1, the increase in the stiffness and the decrease in the ε_f with the increase in *E*/*D* were observed, but there was no significant difference for the σ_{NTf}. This value fell inside around 150, 200, 75 and 30 MPa at 0°, 30°, 60° and 90° of θ, respectively.

Effects of *W*/*D* and *E*/*D* on the σ_{NTf} of cross-ply and angle-ply composites with a pin-loaded joint as a function of θ are presented in Fig. 14. Figure 14(a) illustrated effect of *W*/*D* on the σ_{NTf} for the cross-ply composite laminates with fixed *E*/*D*. It was observed that with the same layup and θ, the σ_{NTf} increased with the decrease in *W*/*D*. In addition, with the same layup and *W*/*D*, the maximum σ_{NTf} was observed at 45° of θ. The result might be that the shear resistance of the fibers was taking the major portion of loading. This value increased from 58.6 MPa to 194.7 MPa when *W*/*D* decreased from 5 to 2. In the case of effect of *E*/*D* as indicated in Fig. 14(b), similar trend can be found with the results of laminates with fixed *E*/*D* (Fig. 14(a)), which the σ_{NTf} was maximum and was symmetric with respect to 45°. In addition, it can be seen that with same layup and θ, the σ_{NTf} of laminates increased with the decrease in *E*/*D*. However, when θ is smaller (say θ < 30°) or larger (say θ > 60°), it was different condition for a laminate with 1 of *E*/*D* compared to the other laminates. Obviously, it can be speculated that the different failure mechanism occurred during these ranges. Even so, the σ_{NTf} of the laminates with different *E*/*D* exhibited

the narrow range from 140 MPa to 200 MPa. Furthermore, when E/D was above 2, no significant difference for the σ_{NTf} of the laminates was observed. Therefore, the result showed that effect of E/D was insignificant on the σ_{NTf} of cross-ply laminates with a pin-loaded joint. Figure. 14(c) shows changes in W/D for the σ_{NTf} of $[(\theta/-\theta)_2]_s$ with fixed E/D. It can be seen that the σ_{NTf} increased with the decrease in W/D. With the same layup and E/D, the maximum σ_{NTf} of laminates occurred during the range of 10° ~ 45° of θ. This phenomenon can be explained that the portion of fibers initiated to endure transverse stress. When θ was during the range of 45° ~ 60°, the σ_{NTf} of laminates decreased with the increase in θ. This phenomenon could be attributed to the decrease in longitudinal stress of fibers because fibers turned in the transverse direction. Above 60° of θ, the σ_{NTf} of laminates leveled off. As shown in Fig. 14(d), effects of E/D on the σ_{NTf} of $[(\theta/-\theta)_2]_s$ with fixed W/D are presented. When θ was below 45°, changes in E/D affect significantly the σ_{NTf} of laminates, especially with 1 of E/D. However, when θ was above 45°, it can be seen that effects of E/D on σ_{NTf} of laminates was insignificant. Conclusively, for $[(\theta/\theta-90)_2]_s$ with different E/D, the optimal θ for failure load is 45°. Additionally, when E/D of $[(\theta/-\theta)_2]_s$ is above 1, there is no significantly difference for σ_{NTf} and the optimal θ is around 30° ~ 45°.

Figures. 15 and 16 show effects of E/D on deformations of $[(45/-45)_2]_s$ with a pin-loaded joint. From numerical analysis in this study, the failure modes of composite laminates can be identified. For $[(45/-45)_2]_s$ with smaller W/D (= 1.5), this layup laminate with 1 or 5 of E/D both seem to occur net-tension failure (Fig. 15). For $[(45/-45)_2]_s$ with larger W/D (= 5), shear-out failure and bearing failure performed in this layup laminate with 1 and 5 of E/D, respectively (Fig. 16). In this study, the results implied that the dimension ratios, especially W/D and E/D, affect significantly the failure mode of composite laminates with a pin-loaded joint. According to this identification, when W/D was beyond 3, it was determined that the transition of the failure mode at a $[(45/-45)_2]_s$ composite laminate.

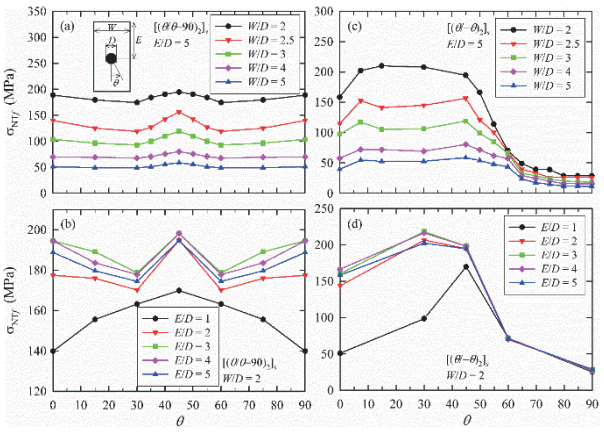

Fig. 14 Effect of W/D and E/D on the net-tension stress at failure of cross-ply and angle-ply composite laminates with a pin-loaded joint as a function of fiber angles (θ)

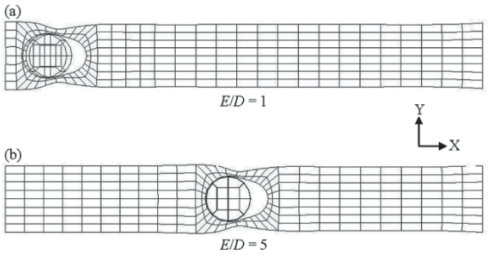

Fig. 15 Effect of E/D on the deformation of $[(45/-45)_2]_s$ with a pin-loaded joint (W/D = 1.5)

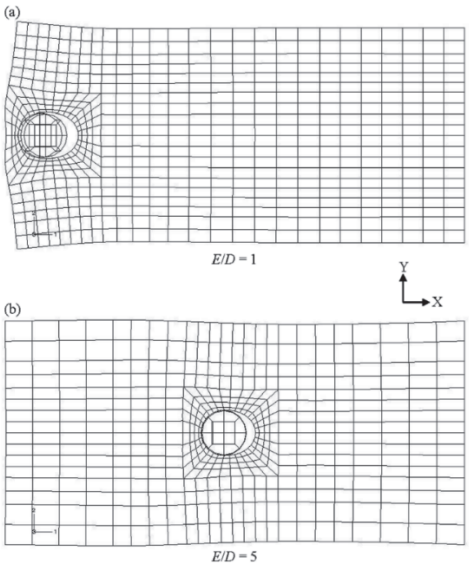

Fig. 16 Effect of E/D on the deformation of $[(45/-45)_2]_s$ with a pin-loaded joint (W/D = 5)

4.2 Effects of Washer Size and Clamping Pressure on Composite Laminates with Pin/Washer-loaded Joints

Figure 17 shows effect of washer size (D_w/D) on load-displacement relations of pin/washer-loaded $[(\theta/-\theta)_2]_s$ with fixed clamping pressure (41.4 MPa). The F_{Pf} and ΔL_{Pf} are defined as the load and displacement at failure of composite laminates with a pin-loaded joint. The F_f and ΔL_f are defined as the load and displacement at failure of composite laminates with pin/washer-loaded joints. For composite laminates with the same θ, its F_f and ΔL_f increased significantly with increase in D_w/D. Especially, the F_f and ΔL_f of the composite laminate with 4 of D_w/D both were both at least 2 times greater than F_{Pf} and ΔL_{Pf}, respectively. This phenomenon could be explained that the resistance of pin-loaded concentration and the ductility both can be improved by adding washers. In addition, the load-displacement curves exhibited the nonlinear behavior when the composite laminates were applied by washer clamping pressure. Also, it can be observed obviously that the ΔL_f of composite laminates with the same D_w/D increased with the increase in θ up to 45°, but no significant difference can be seen for F_f. Furthermore, the maximum F_f and ΔL_f occurred at $[(45/-45)_2]_s$, and the ΔL_f of this laminate with 4 of D_w/D increased by 5.6 times greater than ΔL_{Pf}. It can be calculated that effect of D_w/D has an impact on the ΔL_f more than the F_f.

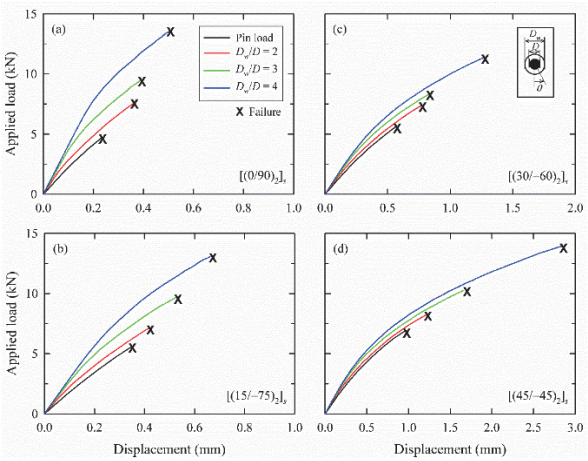

Fig. 17 Effect of washer size on load-displacement relations of angle-ply composite laminates with pin/washer-loaded joints (W/D = 8, E/D = 6, P_{cla} = 41.4 MPa)

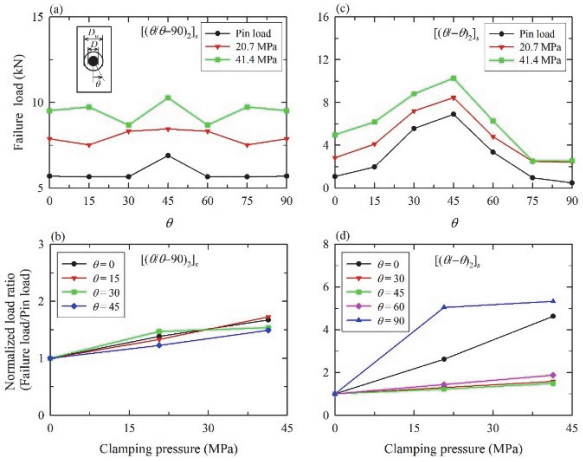

Fig. 18 Effect of clamping pressure on failure loads of cross-ply and angle-ply composite laminates with pin/washer-loaded joints (D_w/D = 3, W/D = 8, E/D = 6)

Figure 18 illustrated that effect of clamping pressure (P_{cla}) on F_fs of cross-ply and angle-ply composite laminates with fixed 3 of D_w/D. For cross-ply $[(\theta/\theta-90)_2]_s$ with the same θ (Fig. 18(a)), the F_f increased with the increase in P_{cla}, and the maximum F_f occurred at $[(45/-45)_2]_s$. From the normalized load ratio (= F_f/F_{Pf}) of $[(\theta/\theta-90)_2]_s$ (Fig. 18(b)), it was calculated to determine the efficiency of P_{cla} on the F_f of composite laminates. The results demonstrated that the normalized load ratio slightly increased to around 1.5 at 41.4 MPa of P_{cla} regardless of θ. For angle-ply $[(\theta/-\theta)_2]_s$ with the same θ (Fig. 18(c)), the F_f showed the similar tendency with conditions of $[(\theta/\theta-90)_2]_s$, which the F_f increased with the increase in P_{cla} and the maximum F_f occurred at 45° of θ. The normalized load ratios during 30° ~ 60° of θ was also similar tendency with conditions of $[(\theta/\theta-90)_2]_s$, which increased slightly to around 1.5 with the increase in P_{cla} (Fig. 18(d)). However, for $[(0/0)_2]_s$ and $[(90/90)_2]_s$, these normalized load ratios increased significantly to 4.6 and 5.3, respectively. Conclusively, influence of P_{cla} on the F_f of $[(\theta/\theta-90)_2]_s$ with all θ was limited, and that of $[(\theta/-\theta)_2]_s$ was also insignificant, except for the small θ (say θ < 30°) and large θ (say θ > 60°).

In the following, effects of D_w/D on the F_f of cross-ply and angle-ply layup laminates with fixed 41.4 MPa of P_{cla} are presented in Fig. 19. From Figs. 19(a) and 19(c), each composites with the same layup and the same θ, the F_fs increased with the increase in D_w/D. As shown in Fig. 19(b), the normalized load ratio of $[(\theta/\theta-90)_2]_s$ with the same θ increased with the increase in D_w/D. In addition, when D_w/D was 4, it can be seen that the F_f was at least twice of the F_{Pf} for all laminates. On the other hand, the normalized load ratio of $[(0/0)_2]_s$ and $[(90/90)_2]_s$ with 4 of D_w/D showed the significant increase to 7.9 and 4.5, respectively (Fig. 19(d)). However, when θ was during 30° ~ 60°, the normalized load ratios of $[(\theta/-\theta)_2]_s$ with 4 of D_w/D have the slight increase to around 2. Above all, it was calculated that effect of D_w/D on the F_f of composite laminates was more significant than effect of P_{cla}.

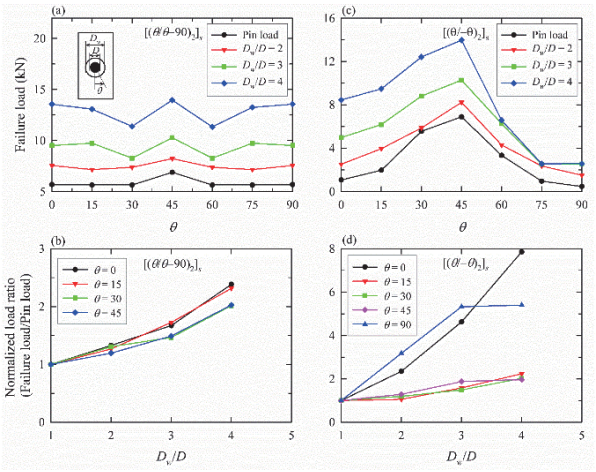

Fig. 19 Effect of washer size on failure loads of cross-ply and angle-ply composite laminates with pin/washer-loaded joints (W/D = 8, E/D = 6, P_{cla} = 41.4 MPa)

5. CONCLUSIONS

In this study, nonlinear FE analyses for composite laminates with pin-filled hole subjected to tensile force and washer clamping pressure were performed. Based on the numerical results, the following conclusions may be drawn:

1. The influence of nonlinear in-plane shear significantly affects the load-displacement curves of composite laminates with $[(\theta/\theta-90)_2]_s$ and $[(\theta/-\theta)_2]_s$ laminate layups. The most significant influence occurred at 45° of θ, and this influence is less significant when θ deviates from 45°.
2. Effects of W/D on the net-tension stress at failure of composite laminates with a pin-loaded joint is more significant, which decreased with the increase in W/D. For $[(\theta/\theta-90)_2]_s$ laminate layups with different W/D, the optimal fiber angle θ for failure load is 45°. For $[(\theta/-\theta)_2]_s$ laminate layups, the optimal fiber angle θ is the range of 7.5° ~ 45°.
3. Effects of E/D on the net-tension stress at failure of composite laminates with a pin-loaded joint are

insignificant, expect for 1of *E*/*D*, but are significant for the strain. For $[(\theta/\theta{-}90)_2]_s$ laminate layups with different *E*/*D*, the optimal fiber angle θ for failure load is 45°. When *E*/*D* of $[(\theta/{-}\theta)_2]_s$ is above 1, there is no significant difference for net-tension stress at failure, and the optimal fiber angle θ is around 30° ~ 45°.

4. From numerical analysis in this study, the failure modes of composite laminates with pin-loaded joint can be identified. According to this identification, it was determined that the transition of the failure mode at a $[(45/{-}45)_2]_s$ composite laminate when *W*/*D* was beyond 3.
5. Effects of Dw/D on the load-displacement relations of composite laminates with pin/washer-loaded joints are more significant. The nonlinear load-displacement curves occur for all composite laminates. In addition, both the failure load and the strain at failure increased with the increase in Dw/D.
6. Effects of Dw/D on failure loads of all layup composite laminates with pin/washer-loaded joints as a function of θ are more significant than effects of P_{cla}. For $[(\theta/\theta{-}90)_2]_s$, the increase in F_f with all of θ was limited. For $[(\theta/{-}\theta)_2]_s$, when θ was the small θ (say $\theta < 30°$) or large θ (say $\theta > 60°$), the F_f significantly increased with the increase in Dw/D.

REFERENCES

1. Camanho, P. P. and Matthews, F. L., "A progressive damage model for mechanically fastened joints in composite laminates," *Journal of Composite Materials*, Vol. 33, No. 24, pp. 2248-2280 (1999).
2. Collings, T. A., "The strength of bolted joints in multi-directional CFRP laminates," *Composites*, Vol. 8, No. 1, pp. 43-55 (1977).
3. Kretsis, G. and Matthews, F. L., "The strength of bolted joints in glass fibre/epoxy laminates," *Composites*, pp. 92-102 (1985).
4. Thoppul, S. D., Finegan, J., and Gibson, R. F., "Mechanics of mechanically fastened joints in polymer–matrix composite structures – a review," *Composites Science and Technology*, Vol. 69, No. 3–4, pp. 301-329 (2009).
5. Camanho, P. P. and Matthews, F. L., "Stress analysis and strength prediction of mechanically fastened joints in FRP: a review," *Composites Part A*, Vol. 28, No. 6, pp. 529-547 (1997).
6. Pisano, A. A. and Fuschi, P., "Mechanically fastened joints in composite laminates: Evaluation of load bearing capacity," *Composites Part B*, Vol. 42, No. 4, pp. 949-961 (2011).
7. Limam, O., Forêt, G., and Zenzri, H., "Ultimate strength of pin-loaded composite laminates: A limit analysis approach," *Composite Structures*, Vol. 93, No. 4, pp. 1217-1224 (2011).
8. Atas, A., Mohamed, G. F., and Soutis, C., "Modelling delamination onset and growth in pin loaded composite laminates," *Composites Science and Technology*, Vol. 72, No. 10, pp. 1096-1101 (2012).
9. Wang, Z., Zhou, S., Zhang, J., Wu, X., and Zhou, L., "Progressive failure analysis of bolted single-lap composite joint based on extended finite element method," *Materials & Design*, Vol. 37, pp. 582-588 (2012).
10. Olmedo, A., Santiuste, C., and Barbero, E., "An analytical model for predicting the stiffness and strength of pinned-joint composite laminates," *Composites Science and Technology*, Vol. 90, pp. 67-73 (2014).
11. Ataş, A., Mohamed, G. F., and Soutis, C., "Effect of clamping force on the delamination onset and growth in bolted composite laminates," *Composite Structures*, Vol. 94, No. 2, pp. 548-552 (2012).
12. Zhou, S., Wang, Z., Zhou, J., and Wu, X., "Experimental and numerical investigation on bolted composite joint made by vacuum assisted resin injection," *Composites: Part B*, Vol. 45, No. 1, pp. 1620-1628 (2013).
13. Kapidžić Z., Nilsson L., and Ansell H., "Finite element modeling of mechanically fastened composite-aluminum joints in aircraft structures," *Composite Structures*, Vol. 109, pp. 198-210 (2014).
14. Lin, W.-P. and Hu, H.-T., "Nonlinear analysis of fiber-reinforced composite laminates subjected to uniaxial tensile load," *Journal of Composite Materials*, Vol. 36, No. 12, pp. 1429-1450 (2002).
15. Lin, W.-P. and Hu, H.-T., "Parametric study on the failure of fiber-reinforced composite laminates under biaxial tensile load," *Journal of Composite Materials*, Vol. 36, pp. 1481-1503 (2002).
16. Hu, H.-T., Yang, C.-H., and Lin F.-M., "Buckling analyses of composite laminate skew plates with material nonlinearity," *Composites: Part B*, Vol. 37, No. 1, pp. 26-36 (2006).
17. Hu, H.-T., Lin F.-M., Liu, H.-T., Hung Y.-F., and Pan, T.-C., "Constitutive modeling of reinforced concrete and prestressed concrete structures strengthened by fiber-reinforced plastics," *Composite Structures*, Vol. 92, No. 7, pp. 1640-1650 (2010).
18. Lesmana, C., Hu, H.-T., Lin, F.-M., and Huang, N.-M., "Numerical analysis of square reinforced concrete plates strengthened by fiber-reinforced plastics with various patterns," *Composites: Part B*, Vol. 55, pp. 247-262 (2013).
19. Lesmana, C. and Hu, H.-T., "Parametric analyses of square reinforced concrete slabs strengthened by fiber-reinforced plastics," *Construction and Building Materials*, Vol. 53, pp. 294-304 (2014).
20. Abaqus Inc. Abaqus analysis user's manuals and example problems manuals, version 6.11 Providence, Rhode Island; 2011.
21. Okutan, B., "The effects of geometric parameter on the failure strength for pin-loaded multi-directional fiber-glass reinforced epoxy laminate," *Composites: Part B*, Vol. 33, No. 8, pp. 567-578 (2002).
22. Hung, C.-L. and Chang, F.-K., "Bearing failure of bolted composite joints, Part II: Model and verification," *Journal of Composite Materials*, Vol. 30, No. 12, pp. 1359-1400 (1996).
23. Hahn, H. T. and Tsai, S. W., "Nonlinear elastic behavior of unidirectional composite laminae," *Journal of Composite Materials*, Vol. 7, No. 1, pp. 102-118 (1973).
24. Jones, R. M. and Morgan, H. S., "Analysis of nonlinear stress–strain behavior of fiber-reinforced composite materials," *AIAA Journal*, Vol. 15, No. 12, pp. 1669-1676 (1977).
25. Tsai, S. W. and Wu, E. M., "A general theory of strength for anisotropic materials," *Journal of Composite Materials*, Vol. 5, No. 1, pp. 58-80 (1971).
26. Narayanaswami, R. and Adelman, H. M., "Evaluation of the tensor polynomial and Hoffman strength theories for composite materials," *Journal of Composite Materials*, Vol. 11, No. 4, pp. 366-377 (1977).
27. Sih, G. C. and Skudra, A. M., *Failure mechanics of composites*, Elsevier Science Publishers, The Netherlands, pp. 71-125 (1985).

108 年 12 月 9 日 收稿
109 年 1 月 22 日 修改
109 年 3 月 16 日 接受